Available online at www.sciencedirect.com
ScienceDirect
Journal of Nuclear Materials 372 (2008) 263–276
journal of nuclear materials
www.elsevier.com/locate/jnucmat

Comparative study of the tritium distribution in metals

A.N. Perevezentsev [a,*], A.C. Bell [a], L.A. Rivkis [b], V.M. Filin [b], V.V. Gushin [b], M.I. Belyakov [b], V.I. Bulkin [b], I.M. Kravchenko [b], I.A. Ionessian [b], Y. Torikai [c], M. Matsuyama [c], K. Watanabe [c], A.I. Markin [d]

[a] *EURATOM/UKAEA Fusion Association, Culham Science Centre, Abingdon OX14 3DB, UK*
[b] *All-Russia Institute of Inorganic Materials, 123060, P.O. Box 369, VNIINM, Moscow, Russia*
[c] *Hydrogen Isotope Research Center, University of Toyama, Gofuku 3190, Toyama 930-8555, Japan*
[d] *State Scientific Center TRINITI, 142190 Moscow Region, Russia*

Received 13 September 2006; accepted 20 March 2007

Abstract

Coupons of stainless steel, Inconel, beryllium, copper and aluminium bronze were exposed to tritium in hydrogen gas mixtures over a wide range of parameters: temperature up to 770 K, pressure from 1×10^{-4} MPa to 0.05 MPa, tritium concentration from 1 at.% to 98 at.%. The tritium concentration on the surface and distribution through the metals were measured using radiography, radioluminography, β-ray induced X-ray spectroscopy and acid etching methods. The effect of metal processing, such as forging, polishing and heat treatment on the tritium distribution was studied along with parameters relating to the exposure of the metal to tritium.

1. Introduction

The knowledge of the tritium content and distribution in construction materials is very helpful for design, maintenance and decommissioning of tritium handling facilities. Metals are the major construction materials used for the equipment of such facilities. Tritium retained in the construction materials determines the rate of tritium outgassing during equipment repair and disassembly. The classification for the disposal of these materials as waste also depends on the tritium concentration and the threshold between low level waste (LLW) and intermediate level waste (ILW) in the UK is 12 MBq/kg for γ- and β-emitters. The route for LLW disposal is well established in the UK, however there is no repository for ILW in the UK and its construction in the future is still the subject of discussion. If such a repository becomes available, the cost of ILW disposal would be nevertheless considerably higher than for LLW. The issue of ILW disposal is of particular importance for future deuterium–tritium burning fusion reactors as their operation will involve processing a large quantity of tritium and will create a larger volume of contaminated metals.

The quantity and distribution of tritium sorbed into metals depends on the chemical composition of the metal, any heat treatment applied and the conditions prevalent at the time of exposure to tritium. From a review of the studies reported in the literature the following conclusions can be drawn. The amount of tritium sorbed into a metal exposed to a tritium/hydrogen gas mixture increases with exposure time. At room temperature, a rapid process of tritium sorption into stainless steel was observed for about 30 days before it slowed down. The quantity of sorbed tritium rises linearly with increasing gas pressure. A highly tritium-enriched layer was observed very near to the surface exposed to tritium. The tritium concentration decreases sharply from the surface to the bulk of the steel, although tritium penetrated into the bulk of stainless steel even at ambient temperature [1–14].

* Corresponding author. Tel.: +33 442 256327; fax: +33 442 256405.
E-mail address: alexander.perevezentsev@iter.org (A.N. Perevezentsev).

0022-3115/$ - see front matter © 2007 Published by Elsevier B.V.
doi:10.1016/j.jnucmat.2007.03.215

Observations that tritium permeation rates at moderate temperatures being much faster than would be expected for classical hydrogen diffusion in metals was also made for metals of hydrogen low-permeability, such as Cu, Al, Au, Be, Mo, W, etc. At temperatures around 300 K those metals exhibited permeability several orders of magnitude higher than the values to be expected from extrapolation of permeation results obtained at high temperatures [15].

The profile of tritium concentration with depth, depicted in Fig. 1, was observed [13] for stainless steel types 304 and 316 exposed to a tritium/hydrogen gas mixture. Three distinguishable regions can be identified in the profile: region I shows tritium trapped in the sub-surface layers of a few micrometers thickness (tritium concentration in this region could be more than two orders of magnitude higher than that in the bulk) [12,13]. Region II presents classical atomic hydrogen diffusion in the crystalline lattice of the metal. Tritium in region III, which extends deeply into the bulk, shows a 'flat' profile and appears to result from the grain boundary diffusion.

Similar, but less complicated, profiles were observed in other studies [2,12] of tritium in stainless steel. The common finding is a deep tritium permeation into metals at room temperature and the tritium-enriched sub-surface layer. These observations, reported in various publications [2,13–17], are thought to be attributable to grain boundary diffusion. The grain boundary diffusion coefficient at temperatures around 300 K may be about eight orders of magnitude higher than the coefficient for classical atomic hydrogen diffusion [13].

The amount of tritium sorbed by metals depends on the chemical form of the tritium, the surface smoothness of the metal, history of the metal prior to exposure to tritium and many other factors. Sorption densities for molecular hydrogen fall within two or three orders of magnitude, while the sorption densities for tritiated water span five orders of magnitude [6]. Tritium has been found to exist in three or more sorption states on the surface of stainless steel and copper that have been exposed to gaseous tritium [2]. However, tritium thermally desorbed from these metals was found mostly in the form of water vapour [1–4,6,12,16–18]. Tritium thermal desorption studies of surfaces exposed to gaseous tritium yield a large preponderance of water vapour on desorption for most metals, if there has been any exposure of the surface to air prior to or after exposure to tritium [3,16]. This is true even for desorption carried out under an inert gas with very low concentration of oxygen and water vapours. The ratio of HTO:HT of approximately 5:1 was observed for desorption in nitrogen or helium in the presence of hydrogen. The ratio of HTO:HT = ≈50:1 was observed for desorption in air [1,16].

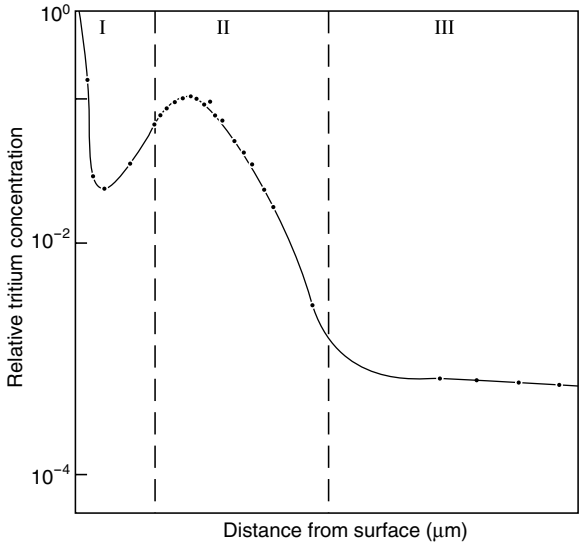

Fig. 1. Tritium depth profile evaluated for stainless steel exposed to hydrogen containing tritium [13].

Under an air atmosphere, the conversion of HT to HTO is promoted on the surfaces of the metal at a temperature above 470 K [16,19]. Even 1 ppm of oxygen in helium is sufficient to oxidise 60% of HT permeating through stainless steel type SS316 at 620 K or higher. Oxygen in quantities of 1000 ppm or higher routinely gave yields of HTO in excess of 98% [16]. Metals also catalyse the isotopic exchange reaction between tritium on the metallic surface and hydrogen containing species in the gas phase. The rate of the tritium isotopic exchange between the water in the gas phase and tritium on the metallic surface was found to be almost independent of the temperature in the range 280–550 K [20].

The operation of the JET machine with tritium plasma [21] led to the sorption of tritium on the vacuum vessel and auxiliary systems. The principal metals used in the JET vacuum vessel and the active gas handling system (AGHS), are grade 316 stainless steel, Inconel 600 and 625, low oxygen copper, beryllium and aluminium bronze. Tritium contamination of the vacuum vessel and AGHS construction materials are expected to vary across a wide range depending on the history of their manufacturing, treatment prior to use and conditions of exposure to tritium. Information helping to predict a possible tritium inventory and distribution in the metals is important for the JET machine maintenance and decommissioning. However, analysis of the level of contamination by withdrawing samples from the operating machine is impractical.

A large number of studies of tritium behaviour in metals have been performed in the past. The samples used in those studies differ in respect of history, treatment prior to exposure and conditions of exposure to tritium. Additionally, different methods of tritium analysis were employed. All these make application of results of those studies for reviewing possible tritium content and distribution in metallic materials of the JET vacuum vessel and the AGHS quite difficult. Therefore the tritium behaviour in the metals present in the JET vacuum vessel and in the AGHS was studied by analysing tritium distribution in the metals

exposed to tritium under applicable plant conditions. The study required a comprehensive analysis of the tritium distribution throughout the metal samples. The number of methods employed so far for tritium measurement in metals is very much limited to non-destructive methods, such as surface activity monitoring [22], spectroscopy of Bremsstrahlung and X-rays induced by interaction of tritium β-decay with materials (BIXS method) [23], and destructive method based on metal dissolution in acids [3,12,18,24]. Non-destructive methods are preferably applied for measuring tritium on the surface of solids. Destructive methods allow analysis of tritium distribution through the sample, but are very labour intensive and produce mixed radioactive and chemically hazardous waste. In this study, a combination of several methods, such as radiography, radioluminography, BIXS and acid etching has been employed for comprehensive analysis of tritium concentration on the surface and its distribution through the bulk of metals.

2. Experiment

2.1. Exposure of metals to tritium

Coupons from SS316L stainless steel, Inconel 600 and 625, beryllium grade 200, oxygen-free copper and aluminium bronze, representing those materials present in the JET vacuum vessel, were used in this study. The chemical compositions of stainless steel and Inconel were within the range established for these alloys. Copper had 0.04 wt% impurities. The main impurities in beryllium were carbon (0.14 wt%), iron (0.08 wt%) and aluminium (0.04 wt%). Aluminium bronze is an alloy of copper with aluminium (10.2 wt%), nickel (5.3 wt%) and iron (4.7 wt%) as main constituents.

Most coupons of stainless steel, Inconel and beryllium were prepared by cutting from a sheet of the material as supplied by the manufacturer. All coupons were of the same size of $100 \times 40\ mm^2$ with a thickness of about 6 mm. Coupons of forged metals were prepared by machining ingots. Some of the stainless steel test coupons were also electropolished at 6×10^4 A min/m^2 in Anopol 65 electrolyte at 323 K. Prior to exposure to tritium, all coupons were cleaned using a method adopted for cleaning of the JET in-vessel components. Some of the coupons were then heated under vacuum at 770 K for 12 h prior to loading with tritium. The coupons were loaded with tritium by exposing to a tritium/hydrogen gas mixture for a period of 8 h. When loading was completed, the coupons were cooled down and the gaseous tritium/hydrogen mixture was evacuated. The coupons were then withdrawn from the apparatus and stored under ambient air. The list of coupons and conditions of their loading with tritium are given in Table 1 which presents also tritium concentrations on the surface and inventories measured using the radioluminography method, as described below.

2.2. Techniques of tritium analysis in metals

Tritium decays and emits β-particles of maximum and average energy of 18 keV and 5.6 keV, respectively. These particles can be detected using various methods. However, due to the low energy the β-particles are quickly absorbed by many materials. For example the depth of mean free path of β-particles of 5.6 keV energy in stainless steel is 0.23 μm only. This makes analysis of tritium distribution in the bulk of metals quite difficult.

2.2.1. Radiography (RG)

A conventional radiography technique has been used to obtain image of tritium distribution on the metal surface. The β-particles emitted by tritium were detected either on photo film of high sensitivity attached to the sample or by using a magnetic microscope. To provide detection of low energy β-particles and to reduce the contribution of Bremsstrahlung, films with a thin top covering layer and a thin layer of photo emulsion were used. Employing a magnetic microscope allowed obtaining images of tritium distribution without direct contact with the sample to be analysed. The vacuum chamber of the microscope, in which samples were installed, was maintained at room temperature and at a residual pressure of 10^{-3} Pa. The tritium distribution in the bulk was evaluated by measuring the tritium depth profiles. This was achieved by measuring the tritium concentrations on the metal surfaces produced by consecutive mechanical removal of thin surface layers using a fine abrasive paper. The tritium depth profile is presented then by tritium concentrations on those surfaces against total thickness of the removed layers.

2.2.2. BIXS

The interaction of electrons with constituent atoms of a material containing tritium generates bremsstrahlung of continuous energy and characteristic X-rays. However, the penetration power of the bremsstrahlung is significantly higher than that of tritium β-particles. For example, the depth of mean free path of bremsstrahlung generated by tritium decay in stainless steel is about 70 μm, which is about 300 times larger than that of the β-particles. The intensity and shape of X-ray spectra generated by tritium in a metal depend on chemical composition of the metal, quantity and distribution of tritium in the metal. In particular, the shape of a spectrum basically reflects the depth profile of tritium. Evaluation of this profile is possible through comparing the measured spectrum with that to be expected for an assumed profile. Assumptions have to be made for the same chemical composition through the metal [23]. While the BIXS technique allows a depth profile evaluation in very small steps, its application for accurate evaluation of profiles which are not of a simple shape (for example shown in Fig. 1) is very time consuming.

Tritium concentrations through the depth of the test coupons were evaluated from bremsstrahlung spectra

Table 1
List of coupons loaded with tritium

Coupon ID[*]	Coupon history[a]			Parameters of exposure to tritium[b]			Tritium concentration[c] (MBq/g)	
	F	P	HT	T (K)	C_T (at.%)	P (MPa)	C_S	C_{AV}
Stainless steel								
S1	F	NP	Yes	470	50 ± 2	0.05	1950	64.6
S2	NF	NP	Yes	470	50 ± 2	0.05	1730	46.9
S3	NF	P	Yes	470	50 ± 2	0.05	1300	33.6
S4[d]	NF	NP	No	300	50 ± 2	0.05	20800	13.1
S6	NF	NP	No	300	50 ± 2	0.05	2380	1.0
S7	NF	P	No	300	50 ± 2	0.05	2220	4.9
S8	NF	P	Yes	300	50 ± 2	0.05	810	0.4
S9	NF	NP	Yes	370	50 ± 2	0.05	1460	3.7
S10	NF	NP	Yes	470	50 ± 2	0.05	1680	46.8
S11	NF	NP	Yes	300	50 ± 2	0.05	1250	1.4
S12	NF	NP	Yes	770	50 ± 2	0.05	7260	923.8
S13	NF	NP	Yes	470	50 ± 2	1E−4	520	3.5
S14	NF	NP	Yes	470	50 ± 2	1E−3	540	5.5
S15	NF	NP	Yes	470	50 ± 2	1E−2	1030	11.7
S16	NF	NP	Yes	470	1.0	0.05	320	1.7
S17	NF	NP	No	470	50 ± 2	0.05	11920	53.2
S18	NF	NP	Yes	470	98.8	0.05	15490	137.3
S19[e]	NF	NP	Yes	470	50 ± 2	0.05	2500	63.8
Inconel								
I1	F	NP	Yes	470	50 ± 2	0.05	2070	17.8
I2	NF	NP	Yes	470	50 ± 2	0.05	2400	53.6
I3[f]	NF	NP	Yes	470	50 ± 2	0.05	2130	117.8
I4	NF	NP	No	470	50 ± 2	0.05	11010	65.5
I5	NF	NP	Yes	300	50 ± 2	0.05	2290	3.3
I6	NF	NP	Yes	370	50 ± 2	0.05	5830	8.4
I7	NF	NP	Yes	570	50 ± 2	0.05	2830	139.5
I8	NF	NP	Yes	770	50 ± 2	0.05	8720	611
Oxygen-free copper								
C1	F	NP	Yes	470	50 ± 2	0.05	5000	1.6
C2	F	NP	No	470	50 ± 2	0.05	22420	5.0
C3[d]	F	NP	No	300	50 ± 2	0.05	10910	5.6
Aluminium bronze								
A1	F	NP	Yes	470	50 ± 2	0.05	3580	14.0
Beryllium								
B1	NF	NP	Yes	300	50 ± 2	0.05	7990	11.6
B2	NF	NP	Yes	470	50 ± 2	0.05	8710	30.4
B3	NF	NP	Yes	570	50 ± 2	0.05	2740	25.8

[*] ID stands for identification number. Several identical coupons with the same ID were prepared and loaded with tritium.
[a] F, NF, P, NP, HT stand for forged, not forged, polished, not polished, heat treatment.
[b] T, C_T, P stand for temperature, tritium concentration and gas pressure during exposure. Usual exposure time was 8 h.
[c] C_S stands for average tritium concentration measured on surfaces exposed to tritium; C_{AV} stands for average tritium inventory of the coupons.
[d] Exposure time was 100 h.
[e] All coupons were made of steel manufactured in the UK, except coupon S19 made of Japanese stainless steel.
[f] This coupon was made of Inconel 625.

measured using a high resolution, low energy silicon-conductor detector of type SS150 and a germanium semi-conductor detector of model GUL0055P, both supplied by CANBERRA. All measurements were carried out at room temperature under the same gas flow rate.

2.2.3. Complete acid dissolution (CAD)

The method measures the total tritium inventory of the sample. Most of the tritium released during metal dissolution remained in the liquid phase. After completion of dissolution, the acids were chemically neutralized and then distilled: tritium in the water distillate was measured by liquid scintillation counting (LSC).

2.2.4. Electrochemical layer-by-layer etching (ELLE)

Removal of a layer of the metal by electrochemical action was performed in a gas-tight electrolytic cell, in which samples of metals loaded with tritium act as an anode. Surfaces that were not etched were coated with a resist. The metals were etched in an aqueous solution of 10 wt% H_2SO_4 at needed rates using a controlled power supply. The gas evolved during the dissolution of the metal

was analysed for tritium; this demonstrated that <1% of the tritium inventory was released into the gas phase.

2.2.5. Radioluminography (RLG)

The application of radioluminography methods for measuring tritium is based on registering photo-stimulated luminescence (PSL) caused by the interaction of tritium β-particles with chemicals on an image plate (IP) [25]. Only particles emitted from a sub-surface layer of thickness less than the mean free path can be detected. The image plates employed in this study were calibrated through exposure to material of known tritium distribution (Amersham International microscales RPA-507 and RPA-510 were used for calibration, they are made from tritiated plastic). The linear correlation between PSL intensity and tritium concentration in the calibration samples was observed for tritium concentrations varying over a three decade range. The effects of duration of the exposure of the image plates to samples and temperature of the image plate on PSL intensity were observed, calibrated and taken into account for the evaluation of tritium concentrations. The interaction of tritium β-particles with the material of the sample analysed causes bremsstrahlung and characteristic X-rays, which are also registered by IP. By measuring the reduction of PSL intensity caused by insertion of a thin polyethylene film (which absorbs the β-radiation) between the IP and the tritium emitting sample, the contribution of the bremsstrahlung and other X-rays was demonstrated to be <0.25%.

The RLG method allows the tritium distribution to be measured along the analysed surface. The image and the PSL intensity for the surface of copper coupon C1 shown in Fig. 2 clearly demonstrate an uneven tritium distribution on grooves of approximately 400 μm size left after machining of the original ingot. Fig. 3 shows an image of the tritium distribution which repeats the shape of the stain left on the surface of coupon S10 after cleaning prior to exposure to tritium. These examples demonstrate the capability of the RLG method to detect changes in tritium concentration caused by defects on the analysed surface. The method employed in this study for cutting the metals provided surfaces of very high quality.

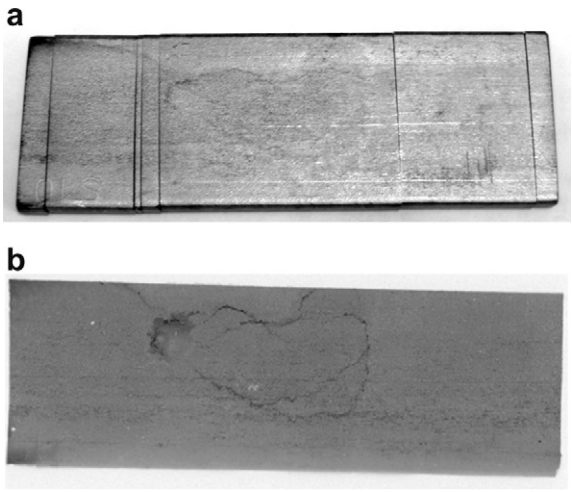

Fig. 3. Photograph (a) and image (b) of the surface of coupon S10 (the image was obtained before the coupon cutting).

For the analysis of the tritium distribution in the bulk, tritium depth profiles were obtained by measuring the tritium distribution on the surface produced by cutting the coupon across. The cutting was performed using a low-speed precision diamond cutter. During the cutting procedure the coupons were cooled with water. The tritium concentration on the surface exposed to tritium and in the region around the cut was measured before and after cutting. Small differences between these two values demonstrated a negligible influence of the cutting procedure on the tritium distribution in stainless steel and Inconel. This was further confirmed by the negligible amounts of tritium found in the water used for cooling the sample during cutting. The effect of cutting on the tritium distribution in copper, beryllium and aluminium bronze was more noticeable, but is acceptably low.

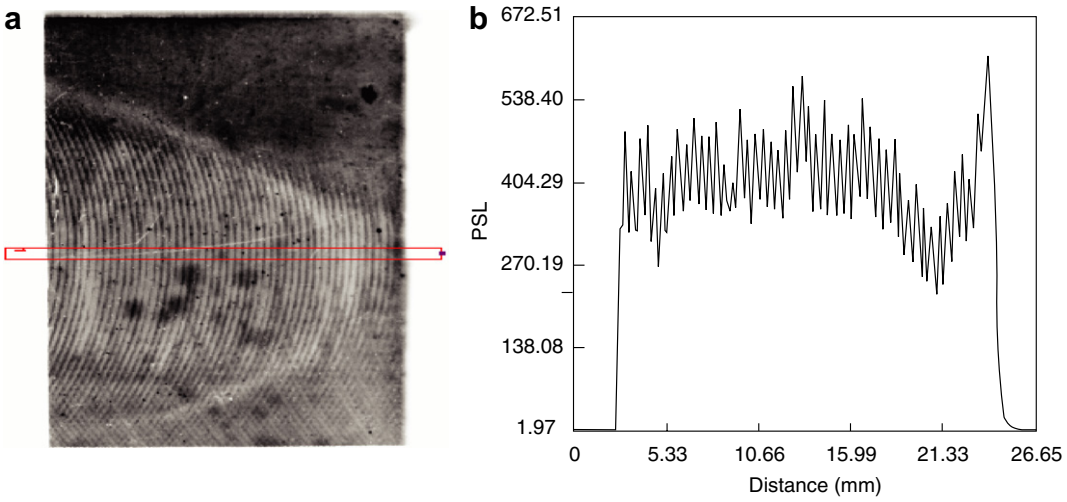

Fig. 2. Light optical image (a) and the PSL intensity distribution (b) for surface of original coupon of copper.

The image plates BAS-TR2025 and image reader BAS-180011 supplied by Fuji, Japan were used in this study. The reader allowed evaluation of images in 50 μm-steps.

The IP can be re-used by irradiation with laser light to remove the image of the sample. The plate requires the protection from tritium contamination and this was done by placing a frame made of 15 μm thickness stainless steel foil in between the IP and sample.

3. Results and discussion

3.1. Tritium concentration on the surface exposed to tritium

Measuring PSL intensities on the same surfaces of different coupons in the course of about 1.5 years of their storage shows that the surfaces exposed to tritium retained fairly constant tritium concentrations that decreased mostly due to tritium decay. The results from measuring tritium concentration on the surface of metals exposed to tritium using the RLG and BIXS methods are given in Tables 1 and 2. Tritium concentrations on two major surfaces of the same coupon varied within ±40%. Table 2 shows that the tritium concentrations measured using different methods for coupons exposed to tritium under the same conditions can differ by up to five times. However, the difference is well within the range of deviations experienced for tritium analysis in metals and is likely to reflect the different nature of the analytical techniques employed and the non-uniform tritium distribution on surfaces. The surface tritium concentrations given in Table 2 show a good qualitative agreement.

In contrast, the PSL intensity on the fresh surface produced during coupon's cutting changes very noticeably in time. This phenomenon is illustrated in Fig. 4. The tritium inventory, which was calculated using the average PSL intensities presented in Fig. 4 and measured at different periods of time elapsed after cutting the surface, rose quickly for the first 50 h. For example, the tritium inventory was evaluated to 46.8, 111 and 165 MBq/g using tritium measurements on the same surface but performed at 4, 24 and 72 h, respectively after the coupon S10 cutting to produce this surface. The tritium migration to the newly produced surface from areas of the metal with larger tritium concentration might be responsible for this phenomenon. However, its mechanism is not fully understood as yet. The study presented here required quantitative comparative tritium depth profiles and inventories in metals loaded with tritium at different conditions. Radioluminography appeared to be the most attractive, among the tested methods, for obtaining information required and for analysing a large number of samples needed. To eliminate the effect of the phenomenon described above on accuracy of presenting tritium distribution in the original coupon, the RLG measurement must be performed immediately after the cut of a coupon. This was not technically possible. However, tritium depth profiles for all the coupons were measured within first the 4 h after the surface was produced. For quantitative comparison purpose the profiles were then normalized to the same reference time of 4 h. To do so, the normalization factors were determined for the coupons S10, I2, C1, A1 and B3. These factors present the ratio of tritium inventory obtained by integration of the depth profile, evaluated for specific time elapsing after the surface production to that of 4 h. For example, dependences of the normalization factors for the coupons S10 and I2

Table 2
Tritium concentration on surfaces exposed to tritium

Sample ID	Tritium concentration on surface[a], C_S (kBq/cm^2)	
	BIXS	RLG
Stainless steel		
S1	670	360
S2	590	320
S3	610	240
S4	4240[b]	3840[b]
S6	1240	440
S7	300	410
S8	440	150
S9	460	270
S10	620	310
S11	330	230
S12	2990	1340
S13	140	96
S14	175	100
S15	280	190
S16	110	60
S17	4160	2200
S18	10 390	2860
S19	650	480
Inconel		
I1	1890	380
I2	1350	440
I3	810	390
I4	4700	2020
I5	2250	420
I6	2990	1070
I7	–	520
I8	2350	1600
Copper		
C1	1630	990
C2	7720	4440
C3	2120	2160
Beryllium		
B1	–	990
B2	–	1080
B3	–	340
Aluminium bronze		
A1	1940	680

[a] The RLG measurement was applied for both major surfaces exposed to tritium of coupons of 100×40 mm^2 size. Using the BIXS method tritium concentrations were measured for four samples of 15×15 mm^2 size produced by cutting from the same coupon of 100×40 mm^2 size. The average concentration, which was calculated using tritium concentrations measured for all the surfaces exposed to tritium and all the samples, is given in Table 2. The measured concentrations deviated from the average one within ±40% range.

[b] The tritium surface concentration of 1780 kBq/cm^2 was measured [26] using a surface activity monitor [22].

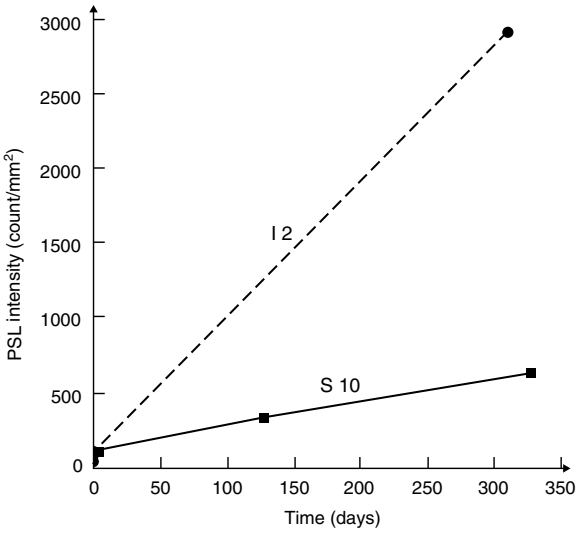

Fig. 4. Averaged PSL intensity measured for cut surfaces of coupons S10 and I2 at different times elapsing after the surfaces production.

can be obtained from the curves in Fig. 4. To obtain normalized tritium concentrations and tritium inventories the measured values were divided by the relevant normalization factor. For example, tritium inventories for the coupon S10 evaluated using measurements carried out at 24 h and 7896 h after the surface production and then normalized gave values of 46.8 MBq/g and 45.4 MBq/g, respectively. These values agree well with the result of 46.8 MBq/g of the measurement undertaken at time of 4 h. The normalization factors determined for coupons S10, I2, C1 and B3 were used for all coupons of stainless steel, Inconel, copper and beryllium. The possible inaccuracy caused by using the same normalization factor for coupons loaded to different tritium inventories and distributions was neglected in this study. Tritium inventories normalized to the reference time of 4 h are listed in Table 1 for all coupons. The tritium inventories obtained by normalization to the reference time of 4 h present values to be larger than those determined by the method of complete dissolution (CAD). This is illustrated in Table 3 which shows that differences between tritium inventories measured using RLG and CAD methods are 23% for coupon S10 and 32% for coupon I2. A larger deviation was observed for copper coupons C1 and the aluminium bronze coupon A1, which were of relatively small tritium inventory.

Table 3
Comparing tritium inventories evaluated using RLG and CAD methods

Coupon number	Tritium inventory (MBq/g)	
	RLG	CAD
S10	46.8	38.0
I2	53.6	40.7
A1	14.0	1.5
C1	1.6	5.0

3.2. Tritium depth profiles

The shape of the tritium depth profile depends mostly on the type of metal and the conditions prevalent at the time of loading with tritium. The profiles in Fig. 5 show that the concentration of tritium increases from the surface down to the sub-surface layer of several hundreds micrometers depth before it decreases further into the bulk of the metal.

Owing to both surfaces of the coupons being exposed to tritium, depth profiles were found to be quite symmetrical, and therefore the profiles shown below are given for a half-thickness of the coupon. However, measuring the same profile could give differing results depending on the method of analysis employed. Fig. 5 shows the full tritium depth profiles through coupon S10 measured using the RLG method. In contrast, tritium depth profiles measured by the RG method for coupon S10, which is illustrated in Fig. 6, but in small steps using mechanical removal of the

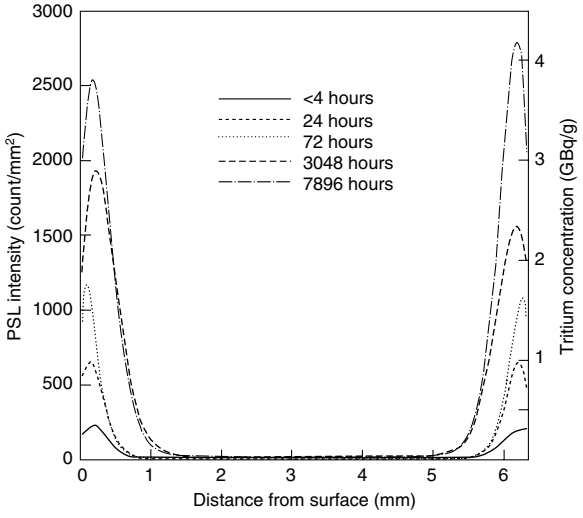

Fig. 5. Tritium depth profiles for coupon S10 measured at different times elapsing after the cut surface production.

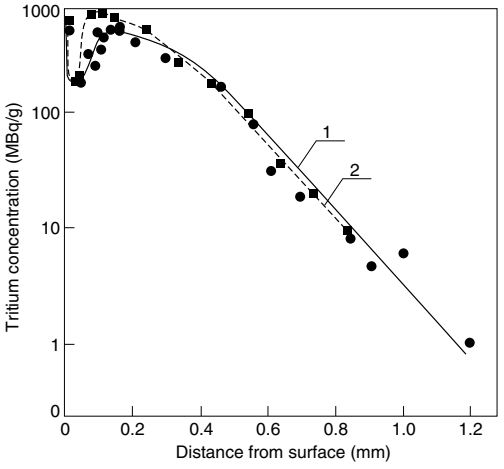

Fig. 6. Tritium depth profiles for coupon S10 measured by radiography (2) and radiography with magnetic microscope (1).

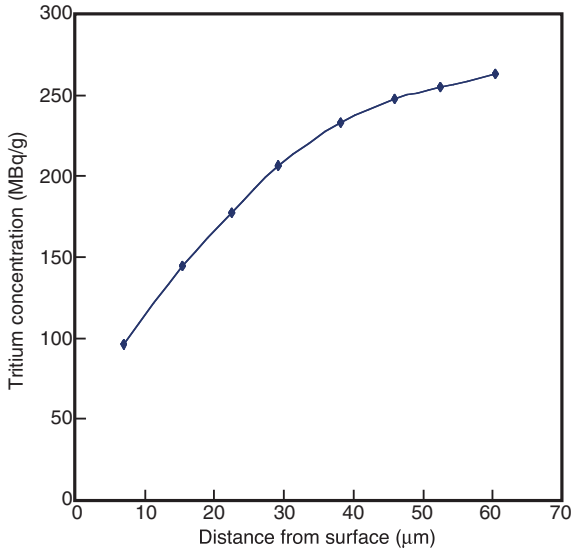

Fig. 7. Tritium depth profile in coupon S10 measured using electrochemical layer-by-layer etching method.

surface layers show the largest tritium concentration on the original surface exposed to tritium. This agrees with the result of RLG measurement given in Table 1 for that surface. The tritium concentration then decreases sharply in a thin sub-surface layer before start rising. Results of BIXS measurements for all tested metals reveal a sharp decrease of tritium concentration in a sub-surface layer of a few micrometers. The tritium depth profile shown in Fig. 7 for the first 60 μm distance from the surface measured for coupon S10 using ELLE method misses this sharp change of tritium concentration in the first micrometers below the surface.

The assessment of tritium depth profiles in coupons of Inconel using the methods given above demonstrated there to be a tritium distribution similar to that of stainless steel. From this we conclude that tritium depth profiles in stainless steel and Inconel are likely to be of shape shown in Fig. 1. Evaluations of the tritium depth profiles by the ELLE method were carried out in consecutive steps with a small time interval between each step. In use of RG method time intervals between production of new surfaces and their analysis were in the order of several days. Taking into account this difference in the procedures and observed effect of tritium concentration rise on a new surface, a good qualitative agreement between tritium concentrations measured in metals using RLG, RG and ELLE methods can be concluded.

Figs. 8 and 9 demonstrate the effect of the concentration of tritium on the surface rising with time after this surface was produced. The maximum tritium concentration rises in layers near to the surface exposed to tritium and layers enriched with tritium become wider. Fig. 8 shows that the maximum tritium concentration on the cut surface of stainless steel rises faster than the average tritium concentration for that surface. Assuming that grain boundary diffusion is the rate determining mechanism of tritium

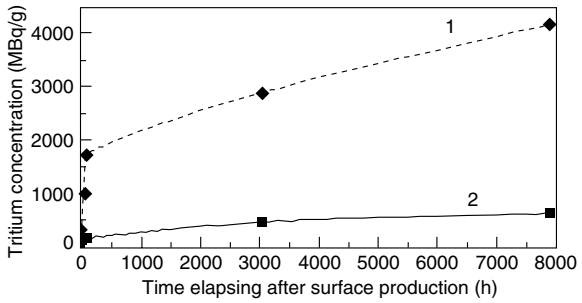

Fig. 8. Maximum (1) and average (2) tritium concentrations measured on the same cut surface of coupon S10.

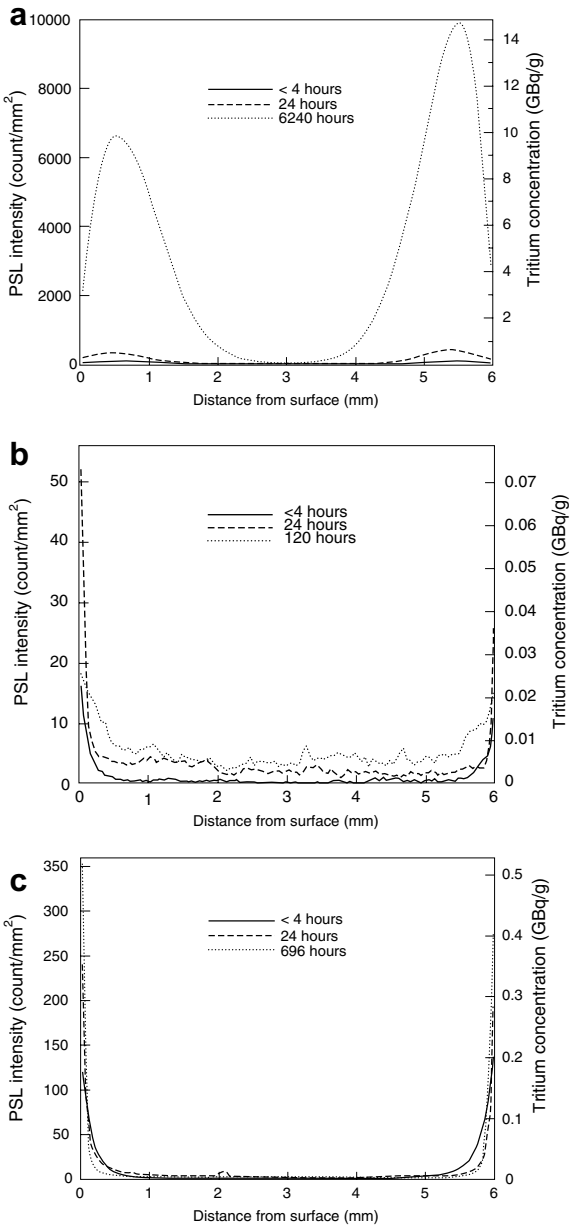

Fig. 9. Tritium depth profiles for coupons I2 (a), C1 (b) and A1 (c) measured at different times elapsing after the cut surface production.

migration in metals at room temperature, the phenomenon illustrated in Figs. 8 and 9 may be explained as follows. Tritium migrates along grain boundaries from thin layers near to the surfaces exposed to tritium (highly enriched with tritium), first to parts of the newly produced surface (which are close to those surfaces) and then tritium is redistributed along that cut surface. Fig. 9 shows this phenomenon for Innconel and copper. Absolute values of the tritium concentration increase on the cut surfaces for aluminium bronze are small.

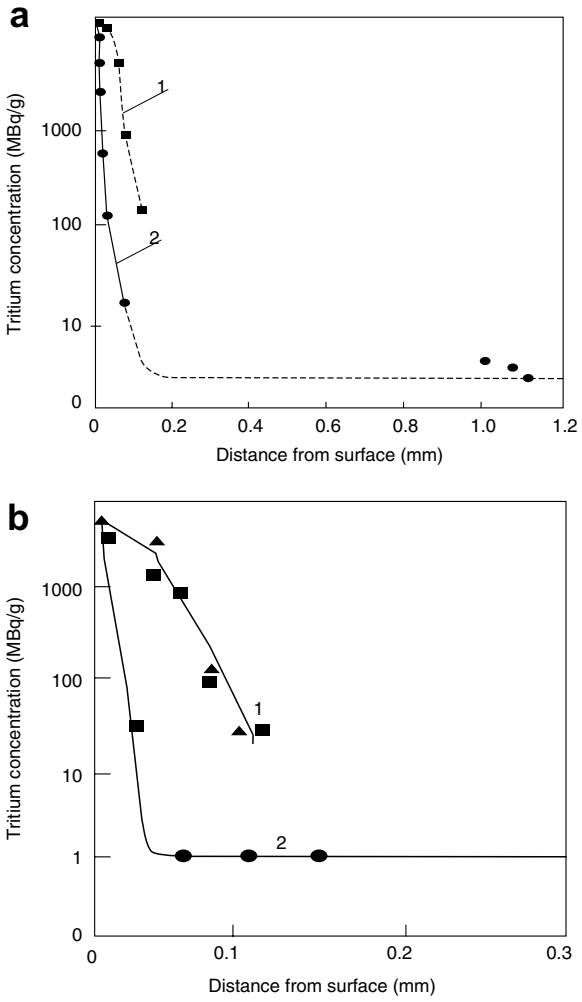

Fig. 10. Distribution of tritium concentration in copper coupon C1 (a) and aluminium bronze coupon A1 (b) measured using radiography (1) and autoradiography with magnetic microscope (2).

Copper, beryllium and aluminium bronze exhibit less complicated tritium depth profiles, which are depicted in Fig. 10, than those of stainless steel and Inconel loaded with tritium at the same conditions. The tritium depth profiles in copper, beryllium and aluminium alloy show a sharp drop of tritium concentration starting from the surface.

The effect of several parameters on content and distribution of tritium in the metals is reviewed below using the profiles measured by the RLG method.

3.3. Metal temperature

Table 4 shows the tritium concentration on the surface and the tritium inventories in the metals loaded with tritium at different temperatures. The temperature effect on the tritium depth profiles is illustrated in Fig. 11.

Review of Table 4 and Fig. 11 shows that the temperature is of small effect on the surface tritium concentration (C_S). Tritium penetrates deeply into the bulk of all tested metals even at room temperature. The sharp rise in tritium inventory (C_{AV}) at temperatures above 370 K might be caused by an increased contribution of atomic hydrogen diffusion into the metal crystalline lattice. This effect is less pronounced for beryllium. The increase of temperature produces a widening of the enriched tritium sub-surface layer and higher tritium concentration in the bulk. Tritium concentrations in the bulk of stainless steel and Inconel loaded with tritium at a temperature of 770 K are higher than in the sub-surface layer of 500 μm thickness, but lower than the surface concentration.

3.4. Duration of exposure

The increase of exposure time from 8 to 100 h at room temperature led to a 9–10-fold rise of the surface concentration and tritium inventory in stainless steel (see coupons S6 and S4 in Table 1). The tritium-enriched sub-surface layer became wider, as illustrated in Fig. 12. According

Table 4
Tritium concentrations in different metals loaded with tritium at different temperatures

Metal	Concentration*	Tritium concentration (MBq/g) Temperature				
		300 K	370 K	470 K	570 K	770 K
Stainless steel	C_S	1270	1420	1680	–	7300
	C_{AV}	1.4	3.7	46.8	–	923.8
Inconel	C_S	2320	5820	2380	2810	8740
	C_{AV}	3.3	8.4	53.6	139.5	611
Beryllium	C_S	8050	–	8690	2780	–
	C_{AV}	11.6	–	30.4	25.8	–

* Tritium concentrations on the surface (C_S) and average tritium concentrations (inventory) for the whole profile (C_{AV}) are given.

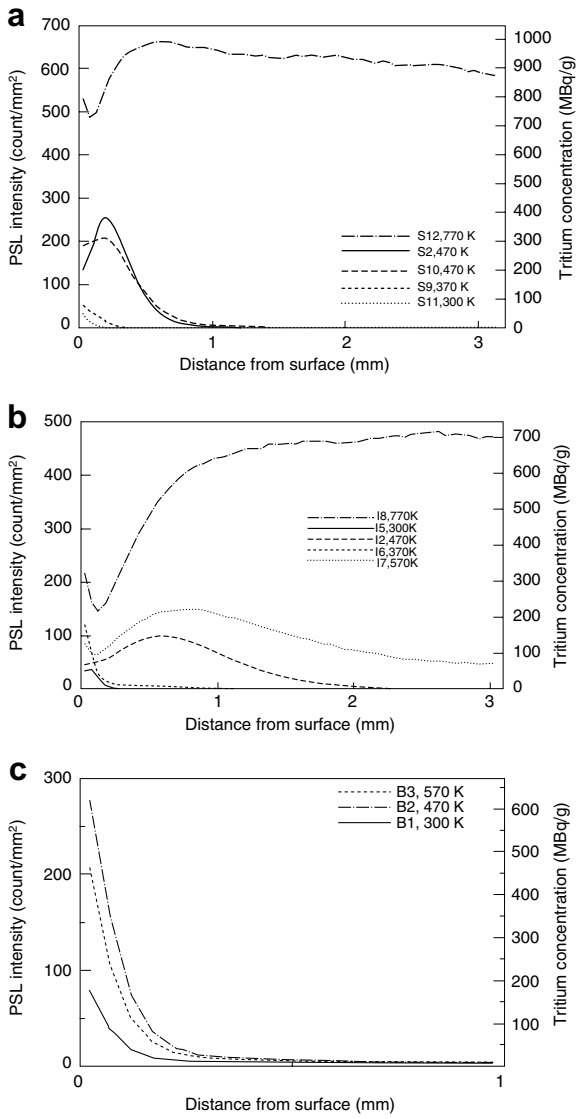

Fig. 11. Tritium depth profiles in coupons of stainless steel (a), Inconel (b) and beryllium (c) exposed to tritium at different temperatures.

to Ref. [2], fast tritium penetration into the bulk of stainless steel at room temperature may continue for about 30 days before it starts slowing down. Tritium profiles in Fig. 12 indicate that if exposure continues then it might be expected that the maximum tritium concentration in the sub-surface layer will be much above the 90 MBq/g measured after a 4 days exposure along with a broadening of the tritium-enriched sub-surface layer. Consequently, exposure to tritium containing hydrogen for a long period of time even at ambient temperature, is likely to heavily contaminate stainless steel and Inconel with tritium from the surface through the bulk.

3.5. Gas pressure

Increasing gas pressure leads to widening of the tritium-enriched sub-surface layer and nearly proportional rise of

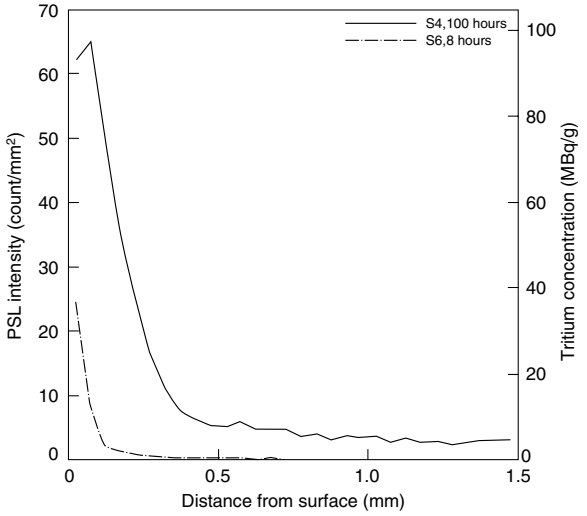

Fig. 12. Tritium profiles in stainless steel exposed to tritium at room temperature for different times.

the surface concentration and tritium inventory, as illustrated in Figs. 13 and 14 for an example of stainless steel. Fig. 14 shows that even a small gas pressure is sufficient for achieving a quite large tritium surface concentration (about 200 MBq/g) and inventory (about 5 MBq/g) in stainless steel after exposure at a temperature of 470 K for 8 h.

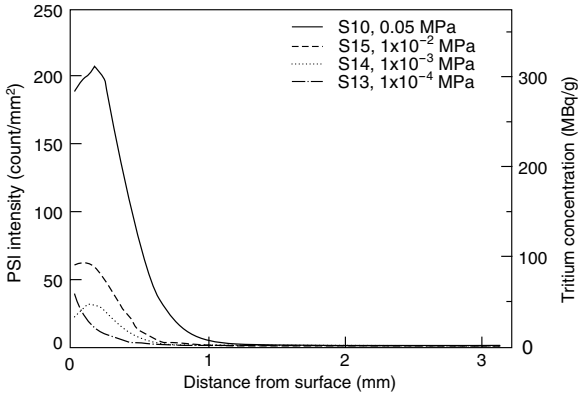

Fig. 13. Tritium depth profiles in stainless steel exposed to tritium at different gas pressures and at 470 K.

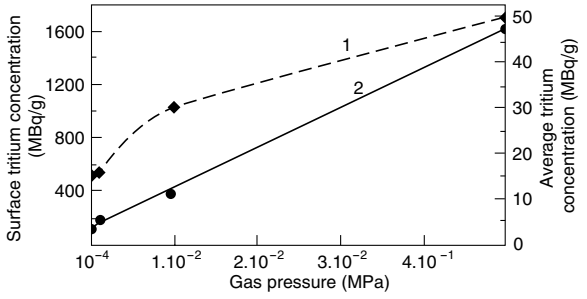

Fig. 14. Effect of gas pressure on surface concentration (1) and tritium inventory (2) in stainless steel.

3.6. Tritium concentration

The increase of tritium concentration in the gas leads to a considerable rise of tritium concentration in stainless steel and to widening of the tritium-enriched sub-surface layer, as illustrated in Table 5 and Fig. 15. The tritium profile for the coupon exposed to nearly pure tritium exhibits a pronounced region I identified in Fig. 1. Table 5 shows that while tritium inventory (C_{AV}) in metal correlates qualitatively with tritium concentration in the gas (C_G), there is no apparent correlation between C_G and C_S.

3.7. Heat treatment prior to loading with tritium

Table 6 and Fig. 16 illustrate the effect of heat treatment on tritium distribution in stainless steel and Inconel. Heat treatment leads to a reduction of the metal surface concentration of tritium, both for polished and non-polished surfaces, when exposed to tritium across a range of temperatures. There is no apparent effect of metal baking on the tritium inventory in the metal. Non-baked stainless steel and Inconel exhibit a pronounced trapping effect of tritium in a sub-surface layer. Baking stainless steel and Inconel prior to exposure to tritium reduces the tritium concentration in the enriched sub-surface layer. This may be due to an increased grain size as a result of the heat treatment causing corresponding decrease in the rate of grain boundary diffusion in baked metal [13,27] and to a reduction in the number of places in the sub-surface layer of baked metal which could be occupied by tritium.

Table 5
Tritium concentration in stainless steel exposed to hydrogen containing different concentrations of tritium

Coupon ID number	Tritium concentration in gas, C_G (vol.%)	Tritium concentration in metal (MBq/g)	
		On surface (C_S)	Inventory (C_{AV})
S16	1	320	1.7
S10	50	1680	46.8
S18	98	15490	137.3

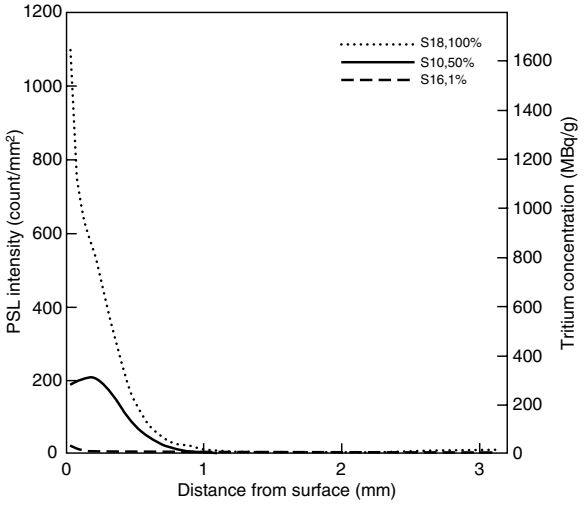

Fig. 15. Tritium depth profiles in stainless steel exposed to hydrogen of different tritium concentrations.

Table 6
Effect of heat treatment on tritium concentration in stainless steel and Inconel

Coupon ID number	Conditions of exposure		Tritium concentration (MBq/g)	
	Temperature (K)	Heat treatment	On surface (C_S)	Inventory (C_{AV})
S6	300	No	2380	1.0
S11		Yes	1250	1.4
S7[a]	300	No	2220	4.9
S8[a]		Yes	810	0.4
S17	470	No	11920	53.2
S10		Yes	1680	46.8
I4	470	No	11010	65.5
I2		Yes	2400	53.6

[a] All coupons were made of non-forged and non-polished metal, except coupons S7 and S8 which were polished prior to exposure to tritium.

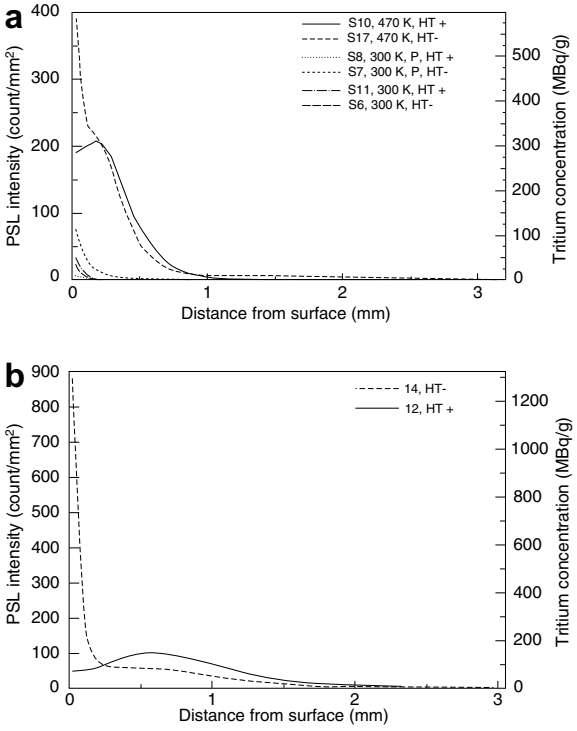

Fig. 16. Tritium depth profiles in stainless steel (a) and Inconel (b) baked (which is market HT+) and not baked (which is marked HT−) under vacuum prior to loading with tritium.

3.8. Polishing of metal surface

Polishing of the surface followed by baking results in a reduction of tritium inventory and surface concentration for steel loaded with tritium at room temperature, as shown in Table 7 for coupons S8 and S11. This effect is

Table 7
Tritium concentrations in polished and non-polished stainless steel

Coupon ID number	T (K)	Polishing	Heat treatment	Tritium concentration (MBq/g)	
				C_S	C_{AV}
S8	300	Yes	Yes	810	0.4
S11		No	Yes	1250	1.4
S7		Yes	No	2220	4.9
S6		No	No	2380	1.0
S3	470	Yes	Yes	1300	33.6
S10		No	Yes	1680	46.8

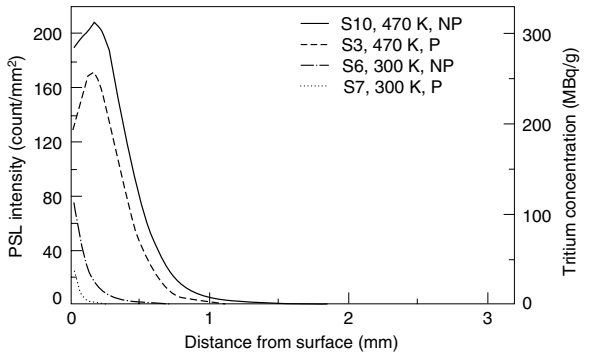

Fig. 17. Tritium depth profiles in stainless steel with surface polished and not polished prior to loading with tritium.

not apparent for non-baked steel (coupons S7 and S6) and steel loaded with tritium at elevated temperature (coupons S3 and S10). Fig. 17 demonstrates that the effect of surface polishing on the width of the tritium-enriched sub-surface layer at different temperatures of exposure to tritium is not very pronounced.

3.9. Metal forging

Comparing the data in Table 1 for tritium inventory and surface concentration in non-forged steel (coupon S10) and Inconel (coupon I2) with those of forged metals (coupons S1 and I1) show that forging has an apparent effect on Inconel only. This is also illustrated in Fig. 18, which shows that forging reduces the tritium concentration in the sub-surface layer which also becomes narrower.

3.10. Chemical composition and manufacturer

Tritium depth profiles given in Fig. 19 show similar tritium distribution in 316L stainless steel produced by the British and Japanese manufacturers. Inconel 625, which is the construction material of the bellows joining the sectors of the JET vacuum vessel inner wall, exhibits a higher tritium inventory and surface concentration than Inconel 600, which is the construction material for the rest of the inner wall. The tritium concentration in the sub-surface layer of Inconel 625 is also larger than that of Inconel 600, although the widths of the layers are the same.

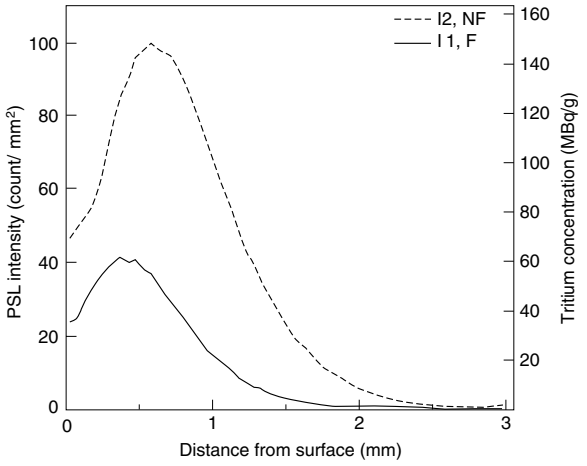

Fig. 18. Tritium depth profiles in Inconel forged and non-forged.

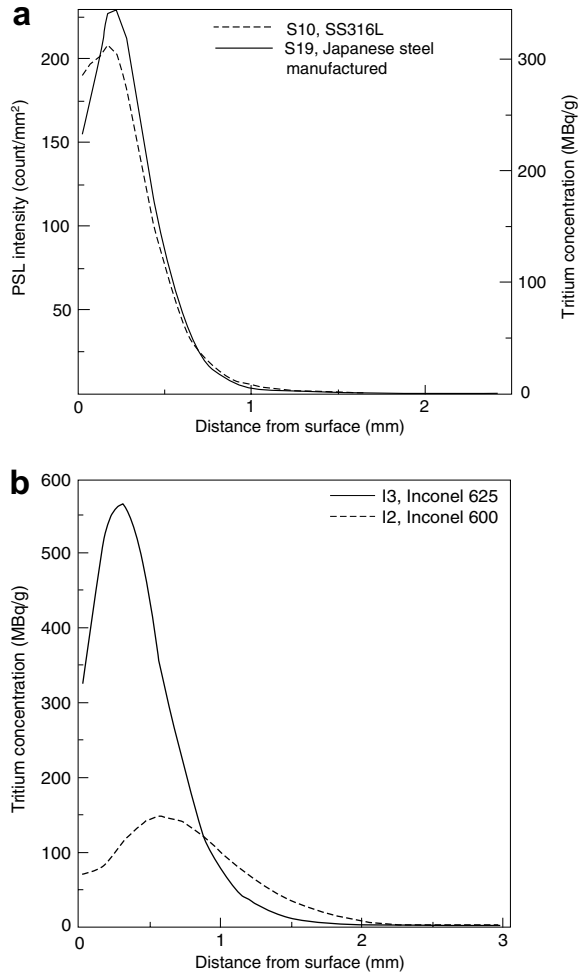

Fig. 19. Tritium depth profiles in stainless steel (a) of British and Japanese manufacturers and in Inconel (b) type 600 and 625.

3.11. Nature of metal

Tritium distributions in different metals exposed to tritium at the same conditions are compared in Table 8 and Fig. 20. The surface tritium concentrations, expressed both

Table 8
Tritium inventories and surface concentrations in metals loaded with tritium at the same conditions

Tritium concentration		Metal				
		Steel (S10)	Inconel (I2)	Copper (C1)	Beryllium (B2)	Aluminium bronze (A1)
C_S (kBq/cm^2)	BIXS	620	1350	1630	–	1940
	RLG	310	440	990	990	680
C_S (MBq/g)	BIXS	3360	7360	8230	–	4940
	RLG	1680	2400	5000	7990	3580
C_{AV} (MBq/g)	CAD	38.1	40.7	5.0	–	1.5
	RLG	46.8	53.6	1.5	30.4	14.0

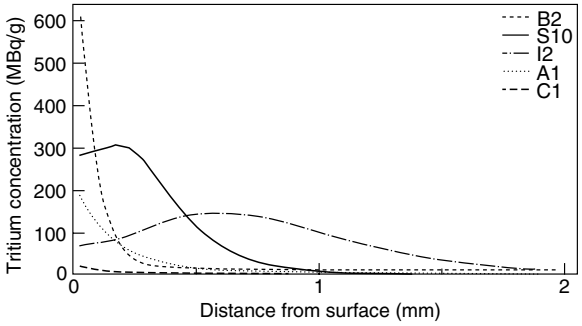

Fig. 20. Tritium depth profiles in different metals loaded with tritium at the same conditions.

per surface area and mass, in beryllium, copper and aluminium bronze are higher than those in steel and Inconel, although their tritium-enriched sub-surface layers are much narrower and have a noticeably less tritium inventory than those of steel and Inconel.

The data presented in Table 8 and Fig. 20 allow some forecast in respect of the decommissioning of the JET vacuum vessel, which has been operated at prolonged temperatures in the range 470–590 K. Metallic waste to be generated from the disassembly of the JET vacuum vessel will contain all the metals listed in Table 8. Inconel 600 and 625 are the major materials of construction of the vacuum vessel. Inconel shows tritium contents higher than those of stainless steel and other metals so it will out-gas with tritium for a longer period of time than other metals. The rate of out-gassing will depend on the rate controlling mechanism under the prevailing temperature and composition of the gas atmosphere. The list of possible mechanisms include recombination and desorption surface reactions, grain boundary migration in the sub-surface layer to the surface and conventional atomic hydrogen diffusion in the crystalline lattice of the metal structure. Predicting the rate of out-gassing is very difficult because all studied metals loaded with tritium at the same conditions exhibit different tritium concentrations on the surfaces, in the sub-surface layers and in the bulk.

4. Summary and conclusions

The shape of tritium depth profiles depends on the nature of the metals and conditions prevalent at their exposure to tritium. All metals studied showed a sub-surface layer of several hundreds micrometers thickness enriched with tritium. In stainless steel and Inconel these sub-surface layers include thin layers close to the surface with a very large tritium concentration. In copper, aluminium bronze and beryllium, the tritium concentration decreases continuously from the surface down to the bulk. The difference in shape of the tritium depth profiles and tritium inventories may reflect contributions from different mechanisms for tritium migration and trapping in metals, such as trapping in defects of crystalline lattice and on grain surfaces, grain boundary diffusion, conventional atomic hydrogen diffusion in crystalline lattice of metals, and others.

The method of radioluminography, which allows quantitative analysis of tritium on the surface and tritium distribution in the bulk of metals without producing mixed radioactive and hazardous waste, was used as the main method for tritium analysis. This method provided a reasonable agreement with other methods, such as BIXS, radiography and acid etchings, also used in this study for tritium analysis in some samples.

The effect of various parameters on the tritium inventory, surface concentration and tritium depth profiles in stainless steel, Inconel, beryllium, copper and aluminium bronze were evaluated using the radioluminography method. The observations allow for several conclusions to be drawn:

1. Tritium penetrates quickly and deeply into the bulk of the metals even at room temperature.
2. Tritium concentration on a new surface produced by cutting the metal increases quickly. This might be caused by tritium migration from the rest of the metal to that surface, however, the mechanism of this phenomenon has not fully understood as yet.
3. Profiles observed for SS316L and Inconel 600/625 are wider than those in copper, aluminium bronze and beryllium loaded with tritium under the same conditions.
4. Increasing the temperature results in a widening of the sub-surface layer enriched with tritium and rise in tritium concentration in the bulk. Tritium concentrations in the bulk of stainless steel and Inconel loaded with tritium at temperature of 770 K were

higher than in the sub-surface layer of 500 μm thickness but were lower than those on the surface.

5. Increasing gas pressure leads to a proportionate increase of tritium inventory in steel and to widening of the tritium enriched sub-surface layer.
6. Increase of tritium concentration in the gas led to a considerable rise in the tritium inventory in the metal and to a widening tritium-enriched sub-surface layer.
7. There is no obvious effect of heat treatment prior to tritium loading on tritium distribution in stainless steel with non-polished surfaces exposed to tritium at temperature around 300 K. Heat treatment of samples with polished surfaces reduces tritium loading even at room temperature. Heat treatment of stainless steel and Inconel with non-polished surfaces considerably reduces the tritium loading at elevated temperature.
8. The effect of metal surface polishing on tritium inventory is relatively small.
9. Forging led to increased tritium inventory in stainless steel without widening of the tritium-enriched sub-surface layer. However, it decreased the tritium inventory in Inconel and narrowed the tritium-enriched sub-surface layer.
10. The tritium concentrations on the surfaces of Inconel and stainless steel, which are the principal construction materials of the JET vacuum vessel and the tritium plant, were lower than those of other metals used for in-vessel components. The tritium inventories were larger for Inconel and stainless steel than for other metals presented in JET vacuum vessel. The widest tritium-enriched sub-surface layers were observed for Inconel followed by stainless steel. Narrowest tritium-enriched sub-surface layers were observed for copper.
11. Metals exposed to tritium in hydrogen for several days at moderate conditions, such as low gas pressure and low tritium concentration in the gas, exhibit quite high tritium inventories and have tritium well distributed through the metal. The resulting level of contamination is very likely to be above LLW/ILW threshold, which is 12 MBq/kg in UK for γ- and β-emitters. It is reasonable to expect that metals exposed to tritium in the JET vacuum vessel and the AGHS are likely to present ILW for disposal during decommissioning.

Acknowledgements

This work was funded by the United Kingdom Nuclear Decommissioning Authority and by the European Communities under the contract of Association between EURATOM and UKAEA. The views and opinions expressed herein do not necessary reflect those of the European Commission.

References

[1] R.A. Surette, R.G.G. McElroy, Fus. Technol. 14 (1988) 1141.
[2] T. Hirabayashi, M. Saeki, J. Nucl. Mater. 120 (1984) 309.
[3] N.M. Masaki, T. Hirabayashi, M. Saeki, Fus. Technol. 15 (1989) 1337.
[4] X. Cao, B. Yang, H. Tan, J. Wan, C. Jiang, Fus. Sci. Technol. 41 (2002) 892.
[5] M. Nishikawa et al., J. Nucl. Mater. 277 (2000) 99.
[6] R.S. Dickson, J. Miller, Fus. Technol. 21 (1992) 850.
[7] A. Perujo, K. Douglas, E. Serra, Fus. Eng. Des. 31 (1995) 101.
[8] J.R. Robins, F.E. Bartoszek, K.B. Woodall, Fus. Technol. 8 (1985) 2455.
[9] J.T. Gill, W.E. Moddeman, R.E. Ellefson, J. Vac. Sci. Technol. A1 (1983) 869.
[10] T. Hirabayashi, M. Saeki, E. Tachikawa, J. Nucl. Mater. 126 (1984) 38.
[11] T. Hirabayashi, M. Saeki, E. Tachikawa, J. Nucl. Mater. 127 (1985) 187.
[12] A. Perevezentsev et al., Fus. Sci. Technol. 41 (2002) 746.
[13] R.D. Calder, T.S. Elleman, K. Verghese, J. Nucl. Mater. 46 (1973) 46.
[14] Y. Torikai, R.-D. Penzhorn, M. Matsuyama, K. Watanabe, J. Nucl. Mater. 329–333 (2004) 1624.
[15] J.L. Mainschein, F.E. McMurphy, V.L. Duval, Fus. Technol. 14 (1988) 701.
[16] R.S. Dickson, Tritium interaction with steel and construction materials in fusion devices. A literature review, Report CFFTP G-9039, AECL-10208, November 1990.
[17] F. Ono et al., Fus. Technol. 28 (1995) 1250.
[18] Y. Toriki, R.-D. Penzhorn, M. Matsuyama, K. Watanabe, Fus. Sci. Technol. 48 (2005) 177.
[19] P.A. Finn, E.H. Van Deventer, Fus. Technol. 15 (1989) 1343.
[20] N. Nakashio, J. Yamaguchi, R. Kobayashi, M. Nishikawa, Fus. Technol. 39 (2001) 189.
[21] Fus. Eng. Des. 47 (1999) 107.
[22] C.R. Shmayda, W.T. Shmayda, N.P. Kherani, Fus. Sci. Technol. 41 (2002) 500.
[23] M. Matsuyama, K. Watanabe, K. Hasegawa, Fus. Eng. Des. 39&40 (1998) 929.
[24] T. Hirabayashi, M. Saeki, E. Tachikawa, J. Nucl. Mater. 136 (1985) 179.
[25] H. Saitoh et al., J. Nucl. Mater. 258–263 (1998) 1404.
[26] W. Shmayda, Personal communication, March 2006.
[27] J.-P. Bacher, C. Benvinuti, P. Chiggiato, et al., Vacuum Sci. Technol. A21 (1) (2003) 167.